Letter

Ultrafast Vibrational Response of Activated C−D Bonds in a Chloroform−Platinum(II) Complex

Jia Zhang, Achintya Kundu, Thomas Elsaesser,* Piero Macchi, Marcel Kalter, Georg Eickerling, and Wolfgang Scherer

Read Online

ACCESS | Metrics & More | Article Recommendations

ABSTRACT: The vibrational response of the activated C−D bond in the chloroform complex $[Pt(C_6H_5)_2(btz-N,N')\cdot CDCl_3$, where btz = 2,2′-bi-5,6-dihydro-4H-1,3-thiazine] is studied by linear and nonlinear two-dimensional infrared (2D-IR) spectroscopy. The change of the C−D stretching vibration of metal-coordinated $CDCl_3$ relative to the free solvent molecule serves as a measure of the non-classical Pt···D−C interaction strength. The stretching absorption band of the activated C−D bond displays a red shift of 119 cm^{-1} relative to uncoordinated $CDCl_3$, a strong broadening, and an 8-fold enhancement of spectrally integrated absorption. The infrared (IR) absorption and 2D-IR line shapes are governed by spectral diffusion on 200 fs and 2 ps time scales, induced by the fluctuating solvent $CDCl_3$. The enhanced vibrational absorption and coupling to solvent forces are assigned to the enhanced electric polarizability of the activated C−D bond. Density functional theory calculations show a significant increase of C−D bond polarizability of $CDCl_3$ upon coordination to the 16 valence electron Pt(II) complex.
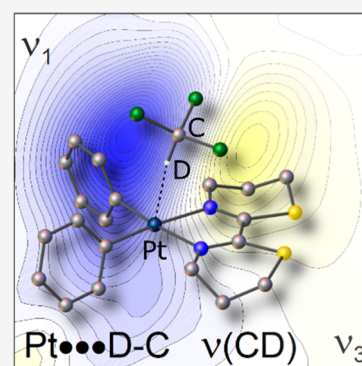
The metal-induced activation of covalent carbon−hydrogen (C−H) bonds plays a key role in many catalytic processes of industrial relevance, such as olefine polymerization. However, the chemical inert nature of C−H bonds as a consequence of their low bond polarizability and large bond dissociation energies renders their activation rather difficult. It is therefore of fundamental interest to understand the electronic origin and the microscopic control parameters of metal-induced C−H bond activation processes in transition metal complexes.

Since the early 1960s, numerous examples of M···H−C interactions have been identified and characterized by a large variety of spectroscopic and structure determination techniques as well as computational methods, e.g., in the case of agostic[1−4] or σ-alkane transition metal complexes.[5,6] However, relatively little information is available in the case of the activation of C−H bonds via metal hydrogen bonding.[7] This is surprising because the first M···H−X hydrogen bonds (X = N and O) have already been observed in metallocenyl alcohols in 1960 by the detection of subtle red shifts of the coordinating M···H−O moieties (M = Fe and Ru) relative to the free hydroxyl stretching modes.[8]

M···H−C hydrogen bonds are considered a predominantly electrostatic three-center four-electron (3c4e) interaction between the hydrogen atom and the metal atom (hydrogen-bond acceptor). As a result of the rather unpolar character of the covalent bond between the carbon atom (hydrogen-bond donor) and the hydrogen atom, 3c4e M···H−C hydrogen bonds are considered to be rather weak. However, as outlined

recently, when the hydrogen-bond acceptor represents an electron-deficient transition metal complex with a valence electron count of ≤16, covalent M···H−C bonding might become the predominant interaction,[9] which causes a significant C−H bond activation with a bond enlargement in the range typically observed in agostic benchmark systems (0.03−0.1 Å).[10,11] This is also the case for our title compound $Pt(C_6H_5)_2(btz-N,N')\cdot CDCl_3$ (**1**), where btz = 2,2′-bi-5,6-dihydro-4H-1,3-thiazine, with 16 valence electrons and a square-planar coordinated d^8−Pt(II) complex center, which is characterized by a significantly depopulated d$_{z^2}$ orbital. The latter can establish a non-classical M···H−C metal hydrogen bond between the metal ligand fragment and the C−H bond of the chloroform ligand.[9]

The M···H−C interaction in compound **1** has been characterized by vibrational spectroscopy because it is particularly sensitive to local molecular interactions, which induce shifts of vibrational transition frequencies and changes of vibrational line shapes. In a very recent study of compound **1**, pressure-dependent infrared (IR) spectra have been measured in the crystalline phase.[9] A broad vibrational
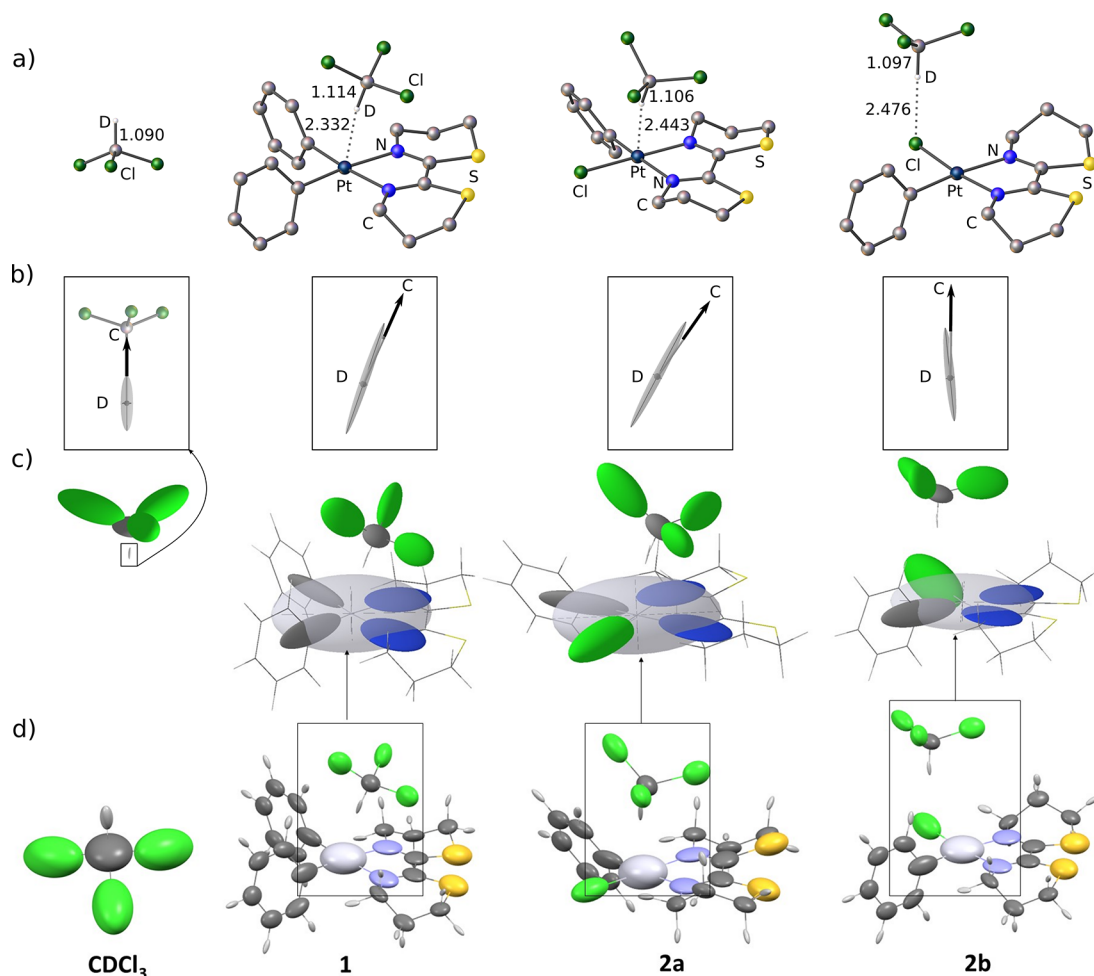
Figure 1. (a) Ball-and-stick representations of the calculated structures of compounds CDCl₃, Pt(C₆H₅)₂(btz-N,N′)·CDCl₃ (**1**), and Pt(C₆H₅)Cl(btz-N,N′)·CDCl₃ (**2a** and **2b**), with salient bond distances given in angstroms. Hydrogen atoms have been omitted for clarity. (b, c, and d) Visualization of the atomic polarizability tensors. Panel d depicts the entire molecules where, for sake of better visibility, the polarizabilities are drawn like thermal ellipsoids using the software Mercury,[17] and therefore, the sizes are not correctly proportioned; however, the orientation is correct. Panel c shows a zoom in the region of the CDCl₃ coordination, and panel b shows a further zoom on the D atoms. Here, the plots are obtained with the software Polaber,[18] and the tensors have the correct proportions, adopting the scale factor of 0.40 Å⁻² (b) and 0.20 Å⁻² (c). Note how the polarizability tensor of D is modified upon passing from uncoordinated to coordinated species. For the sake of clarity in panel b, the principal axes of the D polarizabilities are shown, to emphasize the rotation with respect to the C−D bond direction.

absorption band has been observed, which is red-shifted by 254 cm⁻¹ relative to the C−H stretching band of neat chloroform in the gas phase.[12] This band has been assigned to the C−H stretching vibration of the coordinating chloroform molecule forming a non-classical Pt···H−C bond. We note that the red shift of a C−H band can be used to characterize metal-induced bond activation as a result of agostic or M···H−C hydrogen bonding in solution.[9,13,14]

While the red shift of the C−H stretching frequency can be empirically correlated with a lengthening of the C−H bond,[15] the molecular mechanisms behind the red shift and the strong spectral broadening observed for non-classical M···H−C interactions are not understood. Linear IR spectra reflect the time-averaged vibrational response of the C−H group and do not allow for a clear separation of different broadening mechanisms. In contrast, nonlinear two-dimensional infrared (2D-IR) methods can grasp vibrational frequency correlations on the intrinsic femtosecond time scale of structural fluctuations in liquids and, thus, dynamically discern different contributions to the overall line shape.[16] In this Letter, we report a 2D-IR study of C−D stretching excitations of the

chloroform−Pt(II) complex **1** (Figure 1a) in liquid CDCl₃. The C−D stretching vibration of the CDCl₃ solvent serves as a direct benchmark for bringing out the impact of complex formation on the vibrational properties. In addition to a pronounced red shift and broadening of the C−D stretching band of the complex, we demonstrate a strong enhancement of IR absorption strength in the complex compared to neat CDCl₃. The line shapes of the linear and 2D-IR spectra are governed by spectral diffusion on 200 fs and 2 ps time scales, set by fast structural fluctuations of the solvent. The changes in vibrational line shapes and the strong coupling to solvent fluctuations are assigned to the enhanced electric polarizability of the activated C−D bond.

The molecular structure based on density functional theory (DFT) calculations and a linear IR absorption spectrum of compound **1** are shown in Figures 1a and 2. In the isolated complex, the C−D group of a CDCl₃ molecule coordinates the Pt atom in the axial direction, resulting in a calculated elongation of the C−D bond by 0.024 Å and a respective red shift of the ν(C−D) stretching mode at 2020 cm⁻¹ relative to non-coordinated chloroform [ν(C−D) = 2272 cm⁻¹]. This is
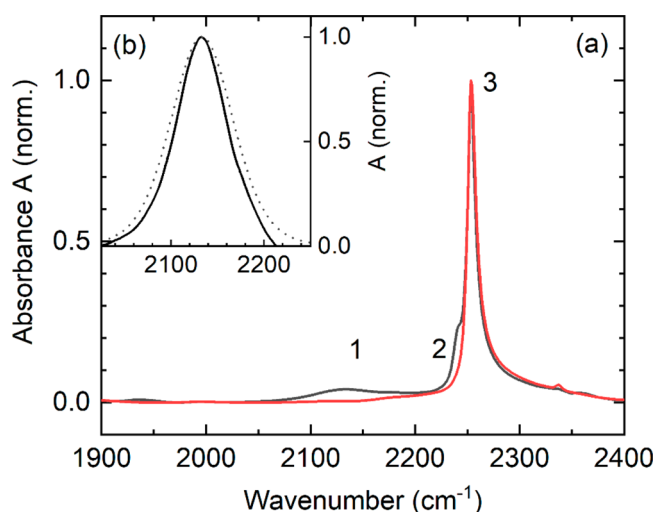
Figure 2. (a) Linear IR absorption spectrum of the complex in CDCl$_3$ (black line, concentration c = 0.24 M), consisting of (1) the stretching absorption band of the complexed C−D groups, (2) a shoulder probably as a result of C−D groups in hydrogen bonds with dissociated btz ligands, and (3) the stretching absorption band of uncomplexed C−D groups. The red line gives the spectrum of the neat solvent CDCl$_3$. Both spectra were normalized to the peak absorbance at 2252 cm^{-1}. (b) Normalized IR absorption in the range of the C−D stretching mode of the complex (1, solid line) and numerical spectrum from the fit of the 2D-IR spectrum (dotted line).

mainly due to the predominant Pt(d$_{z^2}$) → σ*(C−D) back donation and a secondary Pt(RY) ← σ(C−H) donation into unoccupied extravalent ("Rydberg") d orbitals at the metal as revealed by second-order perturbation theory natural bond orbital (NBO) analysis.[9,19] The Pt(d$_{z^2}$) → σ*(C−D) interaction amounts to −26.3 kJ mol^{-1} and provides a substantial contribution to the total bonding energy between the metal ligand fragment and the chloroform ligand (−64.6 kJ mol^{-1}) as derived by an energy decomposition analysis (EDA).[20]

The linear IR absorption spectrum in liquid CDCl$_3$ (black line in Figure 2a) exhibits two prominent components, a broad band centered at 2133 cm^{-1} with a spectral width of 65 cm^{-1} (fwhm) and the much narrower C−D stretching band of the CDCl$_3$ solvent at 2252 cm^{-1} of a spectral width of 12 cm^{-1} only. The assignment of the broad vibrational absorption will be discussed below.

Femtosecond pump−probe measurements give insight in the dynamics of vibrational excitations in the range of the broad IR band. The pump spectrum (dashed line in Figure 3a) is kept below 2220 cm^{-1} to avoid excitation of the solvent via its C−D stretching band at 2252 cm^{-1}. In Figure 3a, we present a series of transient pump−probe spectra recorded at different delay times between pump and probe pulses (colored symbols). The absorption change $\Delta A = -\log(T/T_0)$ in mOD (OD = optical density) is plotted as a function of probe frequency (T and T_0 = sample transmission with and without excitation). The pronounced absorption decrease $\Delta A < 0$ between 2090 and 2220 cm^{-1} is accompanied by an absorption increase $\Delta A > 0$ of similar amplitude at lower probe frequencies. The absorption decrease in the range of the linear absorption band 1 (solid line) originates from the pump-induced depopulation of the $v = 0$ vibrational ground state and stimulated emission on the $v = 1$ to 0 transition. The transient population of the $v = 1$ state gives rise to enhanced absorption
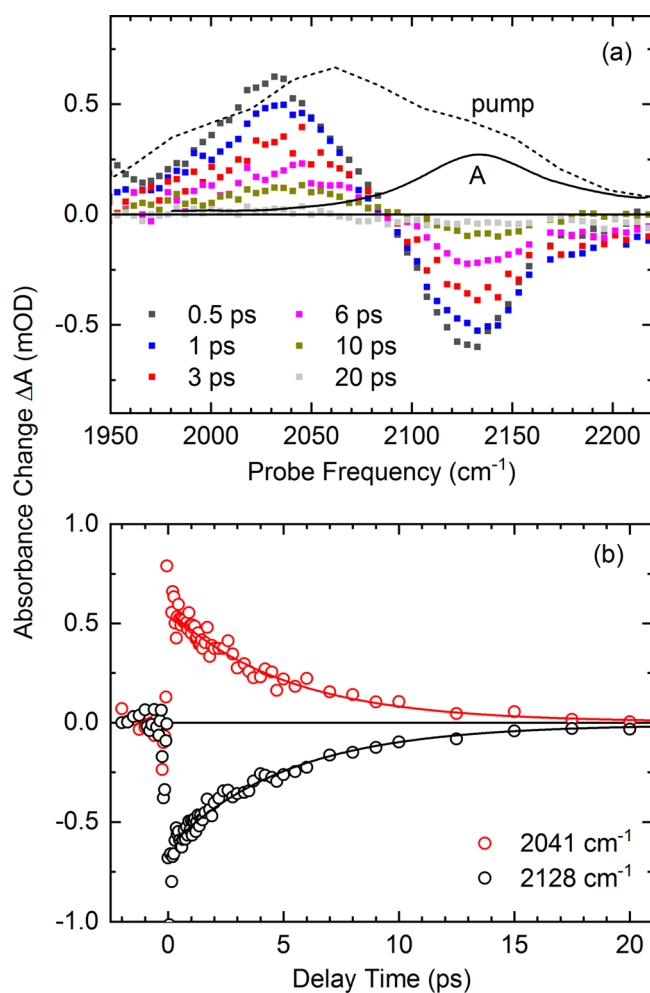

Figure 3. Results from femtosecond pump−probe experiments in the range of the C−D stretching vibration of the Pt(II) complex. (a) Transient pump−probe spectra for different delay times. The absorption change $\Delta A = -\log(T/T_0)$ is plotted as a function of probe frequency (symbols, where T and T_0 = sample transmission with and without excitation). The dashed line represents the spectrum of the pump pulses, and the solid line represents the linear absorption spectrum of the complexes [Pt(C$_6$H$_5$)$_2$(btz-N,N')·CDCl$_3$]. (b) Time-resolved pump−probe traces measured at probe frequencies of 2041 cm^{-1} (red symbols) and 2128 cm^{-1} (black symbols). The absorption change ΔA is plotted as a function of the pump−probe delay. The solid lines are monoexponential fits to the data with a decay time of 5.1 ± 0.3 ps.

on the $v = 1$ to 2 transition, which is anharmonically red-shifted compared to the $v = 0$ to 1 transition. Figure 3b shows two time-resolved transients for fixed probe frequencies of 2041 cm^{-1} ($v = 1$ to 2 transition) and 2128 cm^{-1} ($v = 0$ to 1 transition). Both traces show a quasi-instantaneous rise around delay zero and a complete decay of the absorption changes on a 20 ps time scale. The solid lines are numerical fits to the data points, following a monoexponential decay with a time constant of 5.1 ± 0.3 ps.

More specific insight in vibrational line shapes and the underlying molecular mechanisms is attained from 2D-IR spectra. Figure 4a displays an experimental 2D-IR spectrum, measured at a population time T = 300 fs in the range of the broad absorption band with a maximum at 2133 cm^{-1} (cf. Figure 2). The absorptive 2D signal, i.e., the real part of the sum of the rephasing and non-rephasing signal, is plotted as a
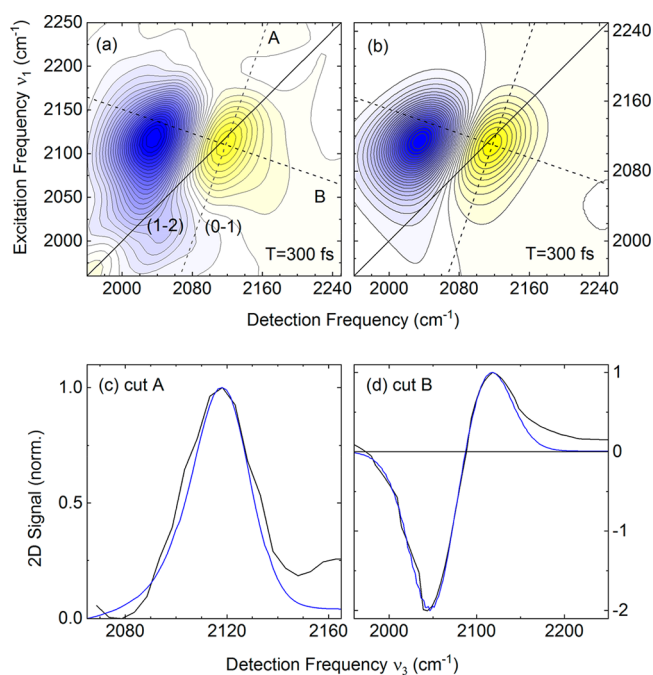
Figure 4. (a) 2D-IR spectrum of the C−D stretching vibration of the Pt(II) complex Pt(C$_6$H$_5$)$_2$(btz-*N*,*N'*)·CDCl$_3$. The absorptive 2D signal measured at a waiting time T = 300 fs is plotted as a function of excitation frequency ν_1 and detection frequency ν_3. Yellow−red contours represent signals on the v = 0 to 1 transition corresponding to an absorption decrease, while blue contours are due to the v = 1 to 2 transition and represent an absorption increase. The signal change between neighboring contour lines is 2%. The dashed lines mark the directions along which the cuts in panels c and (d were taken. (b) Simulated 2D-IR spectrum. (c) Cuts of the 2D-IR spectra along the direction A. The black line represents the experimental data, and the blue line represents the simulation. (d) Same as panel c for a cut along the direction B.

function of the excitation frequency ν_1 (ordinate) and the detection frequency ν_3 (abscissa). The yellow contour represents the 2D signal on the v = 0 to 1 transition, while the blue contour is due to the v = 1 to 2 transition. Following the standard convention of 2D-IR spectroscopy, the yellow contour is given with a positive sign and the blue contour is given with a negative sign, opposite to the sign of the absorption change ΔA in the pump−probe spectra of Figure 3a.

The 2D-IR spectra allow for a clear separation of the signals due to v = 0 to 1 (yellow) and v = 1 to 2 (blue) excitations. The latter are red-shifted along the detection frequency axis ν_3 as a consequence of the anharmonic red shift of the v = 1 to 2 transition. Both components of the 2D signal display elliptic envelopes with the long axis tilted relative to the frequency diagonal $\nu_1 = \nu_3$ (black solid line). For an analysis of the 2D-IR envelopes, cuts along the directions A (diagonal) and B (antidiagonal) are plotted in panels c and d of Figure 4 (black lines).

The 2D-IR spectra were analyzed with the help of a density matrix approach for describing the third-order nonlinear response of the sample.[16,21,22] A three-level system including the v = 0 to 1 transition and the red-shifted v = 1 to 2 transition was considered. To account for the impact of solvent fluctuations on the 2D line shapes, the frequency fluctuation correlation function (FFCF) was approximated by a sum of two Kubo terms.

$$\langle \delta\nu(t)\delta\nu(0)\rangle = \Delta\nu_1{}^2 \exp(-t/\tau_1) + \Delta\nu_2{}^2 \exp(-t/\tau_2)$$

(1)

Here, $\Delta\nu_1$ and $\Delta\nu_2$ are frequency fluctuation amplitudes, and τ_1 and τ_2 with $\tau_1 < \tau_2$ are correlation decay times. On top of the FFCF, the contribution of the v = 1 population decay with a time constant of 5.1 ps was included in the calculations. The calculated 2D-IR spectra were convoluted with the electric field envelopes of the femtosecond mid-IR pulses to facilitate a 1:1 comparison to the experimental data. As a benchmark, the linear IR absorption spectrum of the C−D stretching vibrations was calculated as well (dotted line in Figure 2b).

The 2D-IR spectrum calculated for a population time T = 300 fs is shown in Figure 4b, and the parameter values used in the calculations are summarized in Table 1. The calculated 2D-

Table 1. Parameter Values from the Numerical Simulation of the 2D-IR Spectra

C−D stretching v = 0 to 1 transition	2133 cm^{-1}
C−D stretching v = 1 to 2 transition	2048 cm^{-1}
diagonal anharmonicity	85 cm^{-1}
vibrational lifetime	5.1 ps
frequency fluctuation correlation function (FFCF)	
correlation decay times	τ_1 = 180 fs
	τ_2 = 2 ps
fluctuation amplitudes	$\Delta\nu_1$ = 35 cm^{-1}
	$\Delta\nu_2$ = 21 cm^{-1}

IR and linear absorption spectra are in good agreement with their experimental counterparts. The correlation decay times derived from the calculation are τ_1 = 180 fs and τ_2 = 2 ps, with the fluctuation amplitudes $\Delta\nu_1$ = 35 cm^{-1} and $\Delta\nu_2$ = 21 cm^{-1}. The fast correlation decay makes the predominant contribution to the antidiagonal line width of the 2D spectral envelopes (Figure 4d), while the slow component induces a substantial broadening along the diagonal (Figure 4c). The population decay of the v = 1 state has a minor influence on the observed line shapes. The diagonal anharmonicity of the oscillators, i.e., the difference in frequency of the v = 0 to 1 transition and the v = 1 to 2 transition, has a value of 85 cm^{-1}. It should be noted that 2D-IR spectra of C−D stretching excitations of uncoordinated CDCl$_3$ molecules, i.e., in the range of the strong absorption band at 2252 cm^{-1} (red line in Figure 2b), have been reported in ref 23. They exhibit spectral envelopes oriented parallel to the excitation frequency axis, pointing to ultrafast spectral diffusion and a line shape close to the homogeneous limit. The diagonal anharmonicity derived from the 2D-IR spectra had a value of 67 cm^{-1}.

We now discuss the experimental and theoretical results. The broad IR absorption band with a maximum at 2133 cm^{-1} occurs in a frequency range where the neat solvent CDCl$_3$ is essentially transparent and vibrational bands of Pt(C$_6$H$_5$)$_2$(btz-*N*,*N'*) are absent. We thus assign the broad IR absorption to the C−D stretching mode of CDCl$_3$ molecules being part of the Pt(II) chloroform complex **1**, in line with the assignment of the corresponding C−D stretching band in ref 4. The red shift by 119 cm^{-1} of the broad C−D stretching band relative to that of uncoordinated CDCl$_3$ molecules at 2252 cm^{-1} is due to the attractive Pt···D−C interaction within the complex, lowering the force constant of the C−D stretching vibration. The extent of the red shift is much larger than frequency shifts observed in hydrogen bonds of similar length between a C−H or C−D group and a non-metallic acceptor atom.[23,24] This fact supports

the results of an earlier DFT study suggesting that the red shift in the title complex is mainly due to the pronounced $Pt(d_z^2) \rightarrow \sigma^*(C-H)$ back donation as a signature of non-classical metal hydrogen bonding.[9]

The strength of the red-shifted C−D stretching absorption is substantially enhanced in comparison to the C−D stretching band of the solvent $CDCl_3$. From the IR absorbance at 2133 cm^{-1}, the complex concentration, and the sample thickness, one calculates a peak molar extinction coefficient $\varepsilon(2133\ cm^{-1}) \approx 16\ M^{-1}\ cm^{-1}$, whereas the solvent C−D stretching band displays a peak extinction coefficient of $\varepsilon(2252\ cm^{-1}) = 6.2\ M^{-1}\ cm^{-1}$. Spectral integration over the two bands gives a ratio of the complex to solvent absorption strength per C−D bond of approximately 8.2. This drastic enhancement is a consequence of the modified electronic structure of the C−D groups interacting with the metal atom. We assign it to a strong increase of electric polarizability.

A theoretical study of the polarizability of the activated C−D bonds is in line with this suggestion. Analysis of the calculated atomic polarizability tensor of the bridging deuterium atom of the Pt···D−C moiety ($\alpha_{33} = 6.8$ bohr^3) in compound **1** (Figure 1 and Table 2) reveals a noticeable polarizability enhancement

Table 2. Calculated Polarizability α_{33} of the Deuterium Atom along the Direction of the Maximum Polarizability (Almost Coinciding with the C−D Direction) and Polarizability α_{11} of the Platinum Atom along the Direction of the Lowest Polarizability (Almost Coinciding with the Pt···D Direction for 1 and 2a) for $CDCl_3$, $Pt(C_6H_5)_2$(btz-N,N')·$CDCl_3$ (1), and $Pt(C_6H_5)Cl$(btz-N,N')·$CDCl_3$ (2a and 2b)

molecular system	polarizability of D, α_{33} (bohr^3)	polarizability of Pt, α_{11} (bohr^3)
$CDCl_3$	3.54	
$Pt(C_6H_5)_2$(btz-N,N')·$CDCl_3$ (1)	6.76	23.34
$Pt(C_6H_5)Cl$(btz-N,N')·$CDCl_3$ (2a)	7.01	23.78
$Pt(C_6H_5)Cl$(btz-N,N')·$CDCl_3$ (2b)	5.62	16.63

along the Pt···D direction relative to that in uncoordinated chloroform ($\alpha_{33} = 3.5$ bohr^3). This enhancement is mainly due to the establishment of non-classical Pt···D orbital interactions. Accordingly, the bond polarizabilities of the Pt···D bond of compound **1** and $Pt(C_6H_5)Cl$(btz-N,N')·$CDCl_3$ (compound **2a** in Figure 1) are rather similar (32.4 bohr^3 in compound **1** and 32.3 bohr^3 in compound **2a**) in line with their comparable Pt···D orbital interaction.[9] This is also evident in the α_{11} component of the polarizability tensor of the Pt atom (cf. Table 2), which is very large in compounds **1** and **2a** but significantly smaller in compound **2b**, where no Pt···D interaction takes place.

Also, the C−D bond polarizabilities increase significantly upon establishment of a non-classical Pt···D−C interaction: 8.3 bohr^3 in $CDCl_3$, 14.4 bohr^3 in compound **1**, and 14.5 bohr^3 in compound **2a**. We note that the C−D bond polarizability also increases when $CDCl_3$ is involved in classical hydrogen bonding. However, the polarizability enhancement is smaller. Accordingly, in $Pt(C_6H_5)Cl$(btz-N,N')·$CDCl_3$ (**2b** in Figure 1) characterized by a classical Cl···D−C hydrogen bond,[25] the C−D bond polarizability of the bridging C−D group is 12.2 bohr^3. In this respect, compound **2b** might serve as a benchmark of a classical hydrogen bond, in keeping with the discussion presented by Dos Santos and Macchi.[26] The smaller

C−D bond polarizability in compound **2b** versus compounds **1** and **2a** is also reflected in the smaller atomic polarizability α_{iso} of the chloro ligand in compound **2b** (20.6 bohr^3) compared to those of the platinum atoms in compounds **1** (38.8 bohr^3) and **2a** (36.5 bohr^3). The bond activation itself, however, does not impart a significant change of the bond polarizabilities because small increases in the atom−atom distance affect the polarizability solely in terms of a subtle secondary contribution.

The red shift and absorption enhancement of the C−D stretching band in the complex are accompanied by a strong broadening to a spectral width of 65 cm^{-1} compared to 12 cm^{-1} for the C−D stretching band of $CDCl_3$. The femtosecond pump−probe experiments give a lifetime of the red-shifted C−D stretching vibration of 5.1 ± 0.3 ps, somewhat shorter than the ∼15.7 ps decay time of the C−D vibration at 2252 cm^{-1}.[23] The corresponding lifetime broadening leads to a respective spectral width of 1.04 and 0.35 cm^{-1}, in both cases negligible compared to the total spectral widths. The much stronger broadening is dominated by the impact of fluctuating forces, which $CDCl_3$ solvent molecules in thermal motion exert on the anharmonic C−D stretching oscillators.[27] Such forces originate from short-range dispersion interactions and longer range electric interactions among $CDCl_3$ molecules and with the complex. In neat liquid $CDCl_3$, the molecules display an electric dipole moment of approximately 1.1 D[28,29] and a calculated C−D bond polarizability of 10.4 bohr^3 (calculated using a polarizable continuum model around the molecule of $CDCl_3$; noteworthy, the polarizability of the bond is 8.3 bohr^3 when computed without the polarizable model). Both electric multipole and polarization forces are relevant, which have been approximated by a pairwise additive Coulomb potential and a non-additive polarization energy.

The impact of the fluctuating force on the C−D stretching excitations depends upon the anharmonicity of the C−D stretching oscillator[27,30] and the coupling strength of the C−D bond to the liquid environment. A non-zero diagonal anharmonicity of the oscillator is essential because excursions of the IR transition frequency require a different energy modulation of the two optically coupled states, the $v = 0$ and $v = 1$ states for the fundamental transition. In the present system, the anharmonicities of 67 cm^{-1} for the solvent C−D stretching mode and 85 cm^{-1} for the C−D stretching mode of the complexes are of similar magnitude. The spectral width of the solvent C−D stretching band of 12 cm^{-1} is a measure for the broadening caused by the total fluctuating intermolecular force acting on a non-activated C−D group in the bulk of liquid $CDCl_3$. In striking contrast to this behavior, the spectral width of the C−D stretching band of the complex is roughly 5 times larger. This most interesting and surprising observation points to a substantially stronger coupling to the external fluctuating force. The enhanced electric polarizability of the activated C−D bond thus leads to a significant induced dipole moment of the C−D group, which vice versa results in a stronger coupling to the electric forces from the solvent. We consider this mechanism the main origin of the observed strong broadening.

In our analysis of the linear IR spectrum and the 2D-IR spectrum, the influence of the fluctuating force on the line shapes is described by introducing a FFCF consisting of two Kubo terms (eq 1). The resulting line width is determined by both the frequency fluctuation amplitudes $\Delta \nu_{1,2}$ and the correlation decay times $\tau_{1,2}$. The fluctuation amplitudes are proportional to the coupling strength between the oscillators and their liquid environment, while the correlation times are

determined by the dynamics of thermally activated motions of solvent molecules. The analysis of the 2D-IR line shapes gives decay times of 180 fs and 2 ps in the FFCF and amplitudes of $\Delta\nu_1 = 35$ cm^{-1} and $\Delta\nu_2 = 21$ cm^{-1} for the fast and slower correlation components. The correlation decay times are close to literature values derived from ultrafast Kerr and theoretical studies of chloroform.[28,29,31] The latter have been attributed to orientational and, at short times, collision-induced dynamics. The agreement between the correlation times from the present 2D-IR analysis and literature underlines the prominent influence of fluctuating solvent forces on the vibrational line shape of the C−D vibration of the Pt(II) chloroform complexes. The large fluctuation amplitudes are specific for the C−D stretching mode of a CDCl$_3$ molecule in a complex and result in the substantial line width of the linear IR absorption and 2D-IR spectra. The much smaller spectral widths of IR absorption and 2D-IR spectra of neat CDCl$_3$[23] suggest fluctuation amplitudes of ∼10 cm^{-1}.

In conclusion, a combination of linear and nonlinear 2D-IR spectroscopy gives direct insight in the molecular mechanisms that determine the ultrafast vibrational dynamics and line shapes of stretching vibrations of activated C−D bonds in chloroform−Pt(II) complexes. A one-to-one comparison to the C−D stretching mode of the solvent CDCl$_3$ elucidates and benchmarks the strong enhancement of absorption strength and the strong broadening of the linear and nonlinear vibrational line shapes of the complex. The broadening is dominated by fluctuating electric forces from the solvent CDCl$_3$. The strongly enhanced electric polarizability of activated C−D bonds plays a key role for such spectroscopic properties. In this way, the changes of the electronic structure of the complex induced by pronounced Pt($d_z{}^2$) → σ*(C−H) back donation manifest in vibrational spectra, making them a sensitive probe for this activation mechanism. A similar polarizability behavior is expected to occur also in the case of agostic or σ-type alkane transition metal complexes displaying activated C−H bonds.

■ MATERIALS AND METHODS

Sample Preparation. A solution was prepared in a glovebox by dissolving Pt(C$_6$H$_5$)$_2$(btz-*N*,*N'*) crystallites in CDCl$_3$ (deutero, 99.8%) with a saturated concentration ($c \approx$ 0.24 M). A neat CDCl$_3$ sample was prepared for reference measurements. The sample was held in a demountable liquid cell (Harrick) in between two 1 mm thick CaF$_2$ windows separated by a Teflon spacer of 390 μm thickness. The linear IR absorption spectrum of the Pt(II) complex in CDCl$_3$ and the CDCl$_3$ reference spectrum were recorded with a Fourier transform infrared (FTIR) spectrometer (Bruker Vertex 80, spectral resolution of 1 cm^{-1}).

Femtosecond Mid-IR Pump−Probe Measurements. The two-color mid-IR pump−probe setup has been described in detail in ref 32. The output of an amplified Ti:sapphire laser system (Coherent Libra, center wavelength of 800 nm, pulse duration of <50 fs, pulse energy of 3.5 mJ, and repetition rate of 1 kHz) drives two independent home-built optical parametric frequency converters to generate two tunable mid-IR pulses. The pump and probe pulses were centered at 2061 and 2105 cm^{-1} without spectral overlap with the very strong C−D stretching absorption peak of CDCl$_3$ at 2252 cm^{-1}. The spectral width of the pulses was 170 cm^{-1} [full width at half maximum (fwhm)], the energy of the pump pulses up to 2 μJ. The intensity ratio of pump to probe pulse

was approximately 100. The temporal cross-correlation between pump and probe pulses had a width of 150 fs (fwhm).

The pump and probe pulses are focused onto the sample with a spot diameter of 100 μm. In parallel, a reference probe pulse travels through an unexcited part of the sample to correct for shot-to-shot intensity fluctuations. After interaction with the sample, the probe and the reference pulse are spectrally dispersed in a monochromator and detected with a dual 64-pixel mercury−cadmium−telluride (MCT) double array detector (spectral resolution of 2 cm^{-1}). Complementary pump−probe experiments with the neat solvent CDCl$_3$ were performed under the same experimental conditions. The absorbance change of the neat solvent is subtracted from that of the Pt(C$_6$H$_5$)$_2$(btz-*N*,*N'*)·CDCl$_3$ sample to derive the response of the Pt(II) complexes.

2D-IR Spectroscopy. Heterodyne-detected three-pulse photon echoes are recorded to derive 2D-IR spectra of the Pt(II) complexes. Details of the 2D-IR setup have been presented elsewhere.[21] Femtosecond pulses tunable in the near-infrared (NIR) are generated in a three-stage optical parametric amplifier, employing β-barium borate crystals driven by a commercial Ti:sapphire laser system (Coherent Legend Elite, 800 nm, 80 fs, 3.1 mJ, and 1 kHz). Difference frequency mixing of the near-IR signal and idler pulses in a 0.75 mm thick GaSe crystal generate mid-IR pulses of a 150 fs duration with a center frequency of 2060 cm^{-1} [spectral width (fwhm) of 150 cm^{-1}] and an energy of some of 4.5 μJ.

Two pairs of phase-locked mid-IR pulses with wavevectors (**k**$_1$ and **k**$_2$) and (**k**$_3$ and **k**$_{LO}$) are generated by reflection from diffractive optics. The pulses (**k**$_1$, **k**$_2$, and **k**$_3$) of 0.3 μJ energy each are focused onto the sample in a box-coherent anti-Stokes Raman scattering (CARS) geometry. The third-order photon echo signal is emitted in the phase matching direction (−**k**$_1$ + **k**$_2$ + **k**$_3$ = **k**$_{sig}$) and overlapped with the local oscillator pulse **k**$_{LO}$ transmitted through the sample for heterodyne detection. The heterodyne signal is dispersed by a monochromator and detected by a 64-pixel MCT detector array (spectral resolution of 2 cm^{-1}), defining the detection frequency ν_3. The recorded signal field depends upon the coherence time τ between the first (**k**$_1$) and second (**k**$_2$) pulse and the waiting time T between the second (**k**$_2$) and third (**k**$_3$) pulse. The excitation frequency ν_1 is generated by Fourier transforming the nonlinear signal along the coherence time τ. For proper phasing of the Fourier transform, the nonlinear signal integrated along the excitation frequency ν_1 is fitted to pump−probe spectra measured in the same setup under identical experimental conditions.

DFT Calculations and Atomic Polarizabilities. DFT calculations on the Pt(II) complexes **1**, **2a**, and **2b** and the CHCl$_3$ molecule were performed employing the BP86 density functional in combination with a TZ2P basis set as implemented in the ADF suite of programs.[33−36] Scalar relativistic effects were included within the zeroth-order regular approximation (ZORA),[37−40] and dispersion interactions for compounds **1** and **2a** were treated via the density-dependent dispersion correction.[41] The molecular geometries were relaxed and verified to converge to a local minimum via subsequent frequency calculations. For the calculation of the bond polarizability, field-dependent calculations employing the Gaussian 09 code (BP86/def2TZVP/DKH2)[42−44] have been performed applying an electric field of 0.005 V/Å in positive and negative *x*, *y*, and *z* directions, respectively.[45] From the field-dependent calculations, intrinsic atomic dipole moments

have been extracted via the quantum theory of atoms in molecules (QTAIM) analysis[46] of the resulting electron densities, performed using AimAll.[47] Bond dipole moments have been calculated for QTAIM recognized bonds, using the QTAIM charges, following the scheme proposed by Bader and Keith[48] and modified by Krawczuk et al.[18] The atomic polarizability tensors were calculated via numerical differentiations of the total atomic dipoles, using the software PolaBer.[18] The inherent asymmetry of the atomic polarizabilities is overcome by the symmetrization scheme of Nye.[49] The bond polarizability is calculated as the projection of the atomic polarizabilities along the according bond direction.

■ AUTHOR INFORMATION

Corresponding Author

Thomas Elsaesser − *Max-Born-Institut für Nichtlineare Optik und Kurzzeitspektroskopie, 12489 Berlin, Germany;* ⦿ orcid.org/0000-0003-3056-6665; Email: elsasser@mbi-berlin.de

Authors

Jia Zhang − *Max-Born-Institut für Nichtlineare Optik und Kurzzeitspektroskopie, 12489 Berlin, Germany;* ⦿ orcid.org/0000-0002-9073-3931

Achintya Kundu − *Max-Born-Institut für Nichtlineare Optik und Kurzzeitspektroskopie, 12489 Berlin, Germany;* ⦿ orcid.org/0000-0002-6252-1763

Piero Macchi − *Department of Chemistry, Materials and Chemical Engineering, Politecnico di Milano, 20131 Milano, Italy;* ⦿ orcid.org/0000-0001-6292-9825

Marcel Kalter − *Institut für Physik, Universität Augsburg, 86135 Augsburg, Germany*

Georg Eickerling − *Institut für Physik, Universität Augsburg, 86135 Augsburg, Germany*

Wolfgang Scherer − *Institut für Physik, Universität Augsburg, 86135 Augsburg, Germany;* ⦿ orcid.org/0000-0002-9307-082X

Complete contact information is available at:
https://pubs.acs.org/10.1021/acs.jpclett.2c00771

Notes

The authors declare no competing financial interest.

■ REFERENCES

(1) Brookhart, M.; Green, M. L. H.; Wong, L. L. Carbon Hydrogen Transition-Metal Bonds. *Prog. Inorg. Chem.* **2007**, *36*, 1−124.

(2) Scherer, W.; McGrady, G. S. Agostic Interactions in d[0] Metal Alkyl Complexes. *Angew. Chem., Int. Ed.* **2004**, *43*, 1782−1806.

(3) Brookhart, M.; Green, M. L. H.; Parkin, G. Agostic Interactions in Transition Metal Compounds. *Proc. Natl. Acad. Sci. U.S.A.* **2007**, *104*, 6908−6914.

(4) Scherer, W.; Herz, V.; Hauf, C. On the Nature of β-Agostic Interactions: A Comparison Between the Molecular Orbital and Charge Density Picture. *Struct. Bonding (Berlin)* **2012**, *146*, 159−207.

(5) Hall, C.; Perutz, R. N. Transition Metal Alkane Complexes. *Chem. Rev.* **1996**, *96*, 3125−3146.

(6) Weller, A. S.; Chadwick, F. M.; McKay, A. I. Transition Metal Alkane-Sigma Complexes: Synthesis, Characterization, and Reactivity. In *Advances in Organometallic Chemistry*; Pérez, P. J., Ed.; Academic Press: Cambridge, U.K., 2016; Vol. 66, Chapter 5, pp 223−276.

(7) Brammer, L. Metals and Hydrogen Bonds. *Dalton Trans.* **2003**, 3145−3157.

(8) Trifan, D. S.; Bacskai, R. Metal-Hydrogen Bonding in Metallocene Compounds. *J. Am. Chem. Soc.* **1960**, *82*, 5010−5011.

(9) Schmitz, D.; Kalter, M.; Dunbar, A. C.; Vöst, M.; Fischer, A.; Batke, K.; et al. Pressure-Enhanced C−H Bond Activation in Chloromethane Platinum(II) Complexes. *Eur. J. Inorg. Chem.* **2020**, *2020*, 79−83.

(10) Scherer, W.; Sirsch, P.; Shorokhov, D.; Tafipolsky, M.; McGrady, G. S.; Gullo, E. Valence Charge Concentrations, Electron Delocalization and β-Agostic Bonding in d[0] Metal Alkyl Complexes. *Chem.—Eur. J.* **2003**, *9*, 6057−6070.

(11) Scherer, W.; Herz, V.; Bruck, A.; Hauf, C.; Reiner, F.; Altmannshofer, S.; Leusser, D.; Stalke, D. The Nature of β-Agostic Bonding in Late-Transition-Metal Alkyl Complexes. *Angew. Chem., Int. Ed.* **2011**, *50*, 2845−2849.

(12) Kimoto, A.; Yamada, H. Infrared Spectra of Crystalline $CHCl_3$ and $CDCl_3$. *Bull. Chem. Soc. Jpn.* **1968**, *41*, 1096−1104.

(13) Kazansky, V. B.; Pidko, E. A. Intensities of IR Stretching Bands as a Criterion of Polarization and Initial Chemical Activation of Adsorbed Molecules in Acid Catalysis. Ethane Adsorption and Dehydrogenation by Zinc Ions in ZnZSM-5 Zeolite. *J. Phys. Chem. B* **2005**, *109*, 2103−2108.

(14) McGrady, G. S.; Downs, A. J.; Haaland, A.; Scherer, W.; McKean, D. C. Vibrational Properties of Ethyltitanium Trichloride and its 1,2-Bis(dimethylphosphino)ethane Adduct: Characterisation of Isolated ν(C−H) Modes and Implications for Agostic Bonding. *Chem. Commun.* **1997**, 1547−1548.

(15) McKean, D. C. New Light on the Stretching Vibrations, Lengths and Strengths of CH, SiH and GeH Bonds. *J. Mol. Struct.* **1984**, *113*, 251−266.

(16) Hamm, P.; Zanni, M. *Concepts and Methods of 2D Infrared Spectroscopy*; Cambridge University Press: Cambridge, U.K., 2011.

(17) Macrae, C. F.; Sovago, I.; Cottrell, S. J.; Galek, P. T. A.; McCabe, P.; Pidcock, E.; Platings, M.; Shields, G. P.; Stevens, J. S.; Towler, M.; Wood, P. A. Mercury 4.0: From Visualization to Analysis, Design and Prediction. *J. Appl. Crystallogr.* **2020**, *53*, 226−235.

(18) Krawczuk, A.; Pérez, D.; Macchi, P. J. PolaBer: A Program to Calculate and Visualize Distributed Atomic Polarizabilities Based on Electron Density Partitioning. *Appl. Cryst.* **2014**, *47*, 1452−1458.

(19) Landis, C. R.; Weinhold, F. *The Chemical Bond: Fundamental Aspects of Chemical Bonding*; Frenking, G., Shaik, S., Eds.; Wiley: Weinheim, Germany, 2014; pp 91−120.

(20) Bickelhaupt, F. M.; Baerends, E. Kohn-Sham Density Functional Theory: Predicting and Understanding Chemistry. *Rev. Comput. Chem.* **2000**, *15*, 1−46.

(21) Siebert, T.; Guchhait, B.; Liu, Y.; Costard, R.; Elsaesser, T. Anharmonic Backbone Vibrations in Ultrafast Processes at the DNA−Water Interface. *J. Phys. Chem. B* **2015**, *119*, 9670−9677.

(22) Mukamel, S. Multidimensional Femtosecond Correlation Spectroscopies of Electronic and Vibrational Excitations. *Annu. Rev. Phys. Chem.* **2000**, *51*, 691−729.

(23) Bian, H.; Li, J.; Wen, X.; Zheng, J. Mode-Specific Intermolecular Vibrational Energy Transfer. I. Phenyl Selenocyanate and Deuterated Chloroform Mixture. *J. Chem. Phys.* **2010**, *132*, 184505.

(24) Kwak, K.; Rosenfeld, D. E.; Chung, J. K.; Fayer, M. D. Solute-Solvent Complex Switching Dynamics of Chloroform between Acetone and Dimethylsulfoxide—Two-Dimensional IR Chemical Exchange Spectroscopy. *J. Phys. Chem. B* **2008**, *112*, 13906−13915.

(25) Kalter, M. Strukturelle und Spektroskopische Untersuchungen Nichtklassischer Wechselwirkungen in σ-Hydrosilan- und σ-Trichlormethan-Metallkomplexen. Dissertation, University of Augsburg, Augsburg, Germany, 2021.

(26) Dos Santos, L. H. R.; Macchi, P. The Role of Hydrogen Bond in Designing Molecular Optical Materials. *Crystals* **2016**, *6*, 43.

(27) Oxtoby, D. W.; Levesque, D.; Weis, J.-J. A Molecular Dynamics Simulation of Dephasing in Liquid Nitrogen. *J. Chem. Phys.* **1978**, *68*, 5528−5533.

(28) Chang, T.-M.; Dang, L. X.; Peterson, K. A. Computer Simulation of Chloroform with a Polarizable Potential Model. *J. Phys. Chem. B* **1997**, *101*, 3413−3419.

(29) Elola, M. D.; Ladanyi, B. M. Polarizability Response in Polar Solvents: Molecular Dynamics Simulations of Acteonitrile and Chloroform. *J. Chem. Phys.* **2005**, *122*, 224506.

(30) Stenger, J.; Madsen, D.; Hamm, P.; Nibbering, E. T. J.; Elsaesser, T. Ultrafast Vibrational Dephasing of Liquid Water. *Phys. Rev. Lett.* **2001**, *87*, 027401.

(31) Laurent, T. F.; Hennig, H.; Ernsting, N. P.; Kovalenko, S. A. The Ultrafast Optical Kerr Effect in Liquid Chloroform: An Estimate of the Collision-Induced Contribution. *Phys. Chem. Chem. Phys.* **2000**, *2*, 2691−2697.

(32) Levinger, N. E.; Costard, R.; Nibbering, E. T. J.; Elsaesser, T. Ultrafast Energy Migration Pathways in Self-Assembled Phospholipids Interacting with Confined Water. *J. Phys. Chem. A* **2011**, *115*, 11952−11959.

(33) Becke, A. D. Density-Functional Exchange-Energy Approximation with Correct Asymptotic Behavior. *Phys. Rev. A* **1988**, *38*, 3098−3100.

(34) Perdew, J. P. Density-Functional Approximation for the Correlation Energy of the Inhomogeneous Electron Gas. *Phys. Rev. B* **1986**, *33*, 8822−8824.

(35) te Velde, G.; Bickelhaupt, F. M.; Baerends, E. J.; Fonseca Guerra, C.; van Gisbergen, S. J. A.; Snijders, J. G.; Ziegler, T. Chemistry with ADF. *J. Comput. Chem.* **2001**, *22*, 931−967.

(36) SCM, Theoretical Chemistry, Vrije Universiteit. *ADF 2022.1*; SCM, Theoretical Chemistry, Vrije Universiteit: Amsterdam, Netherlands, 2022; http://www.scm.com.

(37) van Lenthe, E.; Ehlers, A. E.; Baerends, E. J. Geometry Optimization in the Zero Order Regular Approximation for Relativistic Effects. *J. Chem. Phys.* **1999**, *110*, 8943−8953.

(38) van Lenthe, E.; Baerends, E. J.; Snijders, J. G. Relativistic Regular Two-Component Hamiltonians. *J. Chem. Phys.* **1993**, *99*, 4597−4610.

(39) van Lenthe, E.; Baerends, E. J.; Snijders, J. G. Relativistic Total Energy Using Regular Approximations. *J. Chem. Phys.* **1994**, *101*, 9783−9792.

(40) van Lenthe, E.; van Leeuwen, R.; Baerends, E. J.; Snijders, J. G. Relativistic Regular Two-Component Hamiltonians. *Int. J. Quantum Chem.* **1996**, *57*, 281−293.

(41) Steinmann, S. N.; Corminboeuf, C. Comprehensive Benchmarking of a Density-Dependent Dispersion Correction. *J. Chem. Theory Comput.* **2011**, *7*, 3567−3577.

(42) Douglas, M.; Kroll, N. M. Quantum Electrodynamical Corrections to the Fine Structure of Helium. *Ann. Phys.* **1974**, *82*, 89−155.

(43) Hess, B. A. Relativistic Electronic-Structure Calculations Employing a Two-Component No-Pair Formalism with External-Field Projection Operators. *Phys. Rev. A* **1986**, *33*, 3742−3748.

(44) Wolf, A.; Reiher, M.; Hess, B. A. J. The Generalized Douglas-Kroll Transformation. *Chem. Phys.* **2002**, *117*, 9215−9226.

(45) Frisch, M. J.; Trucks, G. W.; Schlegel, H. B.; Scuseria, G. E.; Robb, M. A.; Cheeseman, J. R.; Scalmani, G.; Barone, V.; Petersson, G. A.; Nakatsuji, H.; Li, X.; Caricato, M.; Marenich, A. V.; Bloino, J.; Janesko, B. G.; Gomperts, R.; Mennucci, B.; Hratchian, H. P.; Ortiz, J. V.; Izmaylov, A. F.; Sonnenberg, J. L.; Williams-Young, D.; Ding, F.; Lipparini, F.; Egidi, F.; Goings, J.; Peng, B.; Petrone, A.; Henderson, T.; Ranasinghe, D.; Zakrzewski, V. G.; Gao, J.; Rega, N.; Zheng, G.; Liang, W.; Hada, M.; Ehara, M.; Toyota, K.; Fukuda, R.; Hasegawa, J.; Ishida, M.; Nakajima, T.; Honda, Y.; Kitao, O.; Nakai, H.; Vreven, T.; Throssell, K.; Montgomery, J. A., Jr.; Peralta, J. E.; Ogliaro, F.; Bearpark, M. J.; Heyd, J. J.; Brothers, E. N.; Kudin, K. N.; Staroverov, V. N.; Keith, T. A.; Kobayashi, R.; Normand, J.; Raghavachari, K.; Rendell, A. P.; Burant, J. C.; Iyengar, S. S.; Tomasi, J.; Cossi, M.; Millam, J. M.; Klene, M.; Adamo, C.; Cammi, R.; Ochterski, J. W.; Martin, R. L.; Morokuma, K.; Farkas, O.; Foresman, J. B.; Fox, D. J. *Gaussian 09, Revision C.01*; Gaussian, Inc.: Wallingford, CT, 2016.

(46) Bader, R. F. W. *Atoms in Molecules: A Quantum Theory*; Oxford University Press: Oxford, U.K., 1994.

(47) Keith, T. A. *AIMAll, Version 19.10.12*; TK Gristmill Software: Overland Park, KS, 2012.

(48) Bader, R.; Keith, T.; Gough, K.; Laidig, K. Properties of Atoms in Molecules: Additivity and Transferability of Group Polarizabilities. *Mol. Phys.* **1992**, *75*, 1167−1189.

(49) Nye, J. F. *Physical Properties of Crystals: Their Representation by Tensors and Matrices*; Oxford University Press: Oxford, U.K., 1985.